Regular Article

Abdulrahman I. Alateyah*

Effect of ECAP die angle and route type on the experimental evolution, crystallographic texture, and mechanical properties of pure magnesium

https://doi.org/10.1515/eng-2022-0406
received September 18, 2022; accepted January 12, 2023

Abstract: In the current study, the effect of equal channel angular pressing parameters such as die route type and die angle were studied. Billets of pure magnesium (Mg) were processed successfully through up to 2-passes of different routes, A, Bc, and C, using equal channel angular pressing dies with different internal angles of 90° and 120° at 225°C. The crystallographic texture and microstructural evolution were investigated using electron back-scatter diffraction. The Vickers microhardness and tensile properties were investigated, analyzed, and linked to the microstructure and crystallographic texture as well. The as-annealed condition revealed relatively coarse equiaxed grains coupled with some extra-elongated grains with average grain size of 6.338 μm. Processing through 2-passes formed an ultrafine grain structure and recrystallized fine grains. This decrease in grain size was associated with hardness and tensile strength enhancement as compared with the as-annealed Mg counterpart. ECAP processing through the 90° die revealed that 2-passes of route Bc was more effective in grain refinement compared to routes A and C, and it reduced the average grain size by 76.45% compared to the as-annealed counterpart. On the other hand, for the ECAP die with 120°, route A was more effective in grain refinement compared to the other routes. Processing through 2-passes of route C resulted in a stronger texture compared to the other routes with momentous rotation for the texture components. Processing of 2-A, 2-Bc, and 2-C through the 90°-die revealed an increase in the Vickers Hardness (HV) of 76.9, 96, and 84.6%, respectively, compared to the AA counterpart. In addition, the tensile findings revealed that the 90°-die resulted in higher ultimate tensile strength coupled with a drop-in ductility compared to the 120°-die. Furthermore, ECAP processing through the 90°-die led to improvement in the ultimate tensile strength by 14.1, 38.4, and 43.75%, respectively, coupled with improving the Mg ductility by 80.9, 73.5, and 47.6% through processing via 2-A, 2-Bc, and 2-C, respectively, compared to the as-annealed counterpart.

Keywords: severe plastic deformation, equal channel angular pressing, route type, pure magnesium, microstructural evolution, crystallographic texture, mechanical properties

1 Introduction

Magnesium (Mg) alloys are ultralight alloys because of their superior specific strength. Mg alloys' densities are about one-quarter that of steel and two-thirds that of aluminum while still providing adequate strength for a variety of applications [1–3]. Furthermore, they exhibit properties such as good recyclability, high-specific stiffness, and great strength-to-weight ratio [4–6], which make them desirable materials for transportation industries with automotive and aerospace applications [7–9]. Additionally, the replacement of traditional materials in automotive with Mg alloys is a prospective proposal for reducing the emission of carbon dioxide as well as decreasing fuel consumption; it was estimated that reducing a car's weight by 10% results in fuel savings of 5–10% [10]. However, the biggest setback to the implementation of Mg-based alloys is their lack of formability, which hinders their performance in automobile applications.

Mg has a hexagonal close-packed (HCP) crystal structure. This severely limits its ductility as a result of the low number of deformation modes characterizing that crystal structure [11]. The HCP crystal structure's brittleness comes from the fact that the structure's slip systems have substantially different critical resolved shear stresses (CRSS) [5,12–14]. As a direct result, Mg alloys perform poorly when worked on at room temperature using common forming techniques, such as rolling and extrusion, and tend to fail [15]. Hot working provides an escape from the inevitable

* **Corresponding author: Abdulrahman I. Alateyah,** Department of Mechanical Engineering, College of Engineering, Qassim University, Unaizah, 56452, Saudi Arabia, e-mail: a.alateyah@qu.edu.sa

failure of Mg at room temperature because the heat increases the alloy's deformability. However, the phenomena of dynamic recovery and recrystallization stunt the desirable effects of strain hardening [16–18]. A plethora of studies and investigations attempted to engineer Mg alloys free of their well-known shortcomings, offering great strength, ductility [19,20], and better corrosion resistance [20,21]. One such approach was the usage of plastic deformation to control the texture, thus mitigating many of Mg alloys' well-known problems.

Severe plastic deformation (SPD) techniques are one of the few suitable methods for metalworking of Mg alloys [22–28]. SPD includes several methods for application to a variety of materials, such as twist extrusion [29], equal channel angular pressing (ECAP) [30–34], multichannel spiral twist extrusion [35–38], accumulative rolling bonding [39], and high-pressure torsion [40–44]. Among the numerous SPD techniques, ECAP has unique features, such as producing an ultrafine grain (UFG) structure, efficient production of nanostructures in alloys, and applicability to industry [45–48].

In recent years, several investigations were launched into the process parameters of ECAP and its influence on the material behavior. The evolved microstructural and mechanical properties of the ECAPed sample are heavily dependent on the plastic deformation degree and form during processing. Therefore, investigating the strain development phenomena is crucial in the design of the ECAP process. The equivalent strain (ε_{eq}) can be determined theoretically based on the die geometry by equation (1) [22,33,48]. The strain is mainly affected by the outer corner angle (Ψ), the internal channel angle (ϕ), and the number of passes (N);

$$\varepsilon_{eq} = \frac{N}{\sqrt{3}} \left[2\cot\left(\frac{\varphi + \Psi}{2}\right) + \Psi\operatorname{cosec}\left(\frac{\varphi + \Psi}{2}\right)\right]. \quad (1)$$

ECAP is the most effective SPD technique that refines metallic materials' grains the most effective out of all the other SPD approaches and hence improving both the mechanical properties. It is important to mention that the strain extent and distribution in ECAP depends on the rotation of the rod about its longitudinal axis. The common ECAP routes are route A, route Bc, route C, and route B_A. Figure 1 illustrates the differences among the different routes. The orientation of the rod in route A remains as is between subsequent passes. However, in route Bc, the rod is rotated 90° between the subsequent passes in the same direction, whereas in route C the sample is rotated 180° (between the subsequent passes) and in route B_A the sample is rotated 90° in opposite direction after each ECAP pass [49]. Additionally, research shows that varying the ECAP routes and using multiple passes further influence the grain refinement and are encouraged to provide improved results. The shear plane direction is also heavily affected by these changes and varies throughout the process [50]. Further research shows that the compressive mechanical properties of ECAPed pure Mg at room temperature using an internal channel angle ϕ = 90° and route Bc became worse and fell off after two passes. Analysis concludes that the newly evolved texture was a major cause of that drop-in properties as well as the activation of non-basal slipping systems. Nevertheless, after the fourth pass, the mechanical properties increased because of grain refinement [51].

The effect of ECAP route type and ECAP channel angle were studied in earlier research. Venkatachalam et al. [52] reported that the ECAP process applied on AA2014 through route Bc manifested significant improvement in mechanical properties, hardness, and strength compared to routes A, C, and Ba, which was argued to be a result of the homogenized effective strain in all the planes. Alateyah et al. [28] had investigated the effect of ECAP route types A, Bc, and C on the microstructural and texture evolution and corrosion behavior of the Mg alloy ZK30. They reported that route type Bc is the most effective in grain refinement, and hence, improves the corrosion rate, whereas both routes A and Bc revealed an improved corrosion resistance with nearly identical values. Alateyah et al. [22,26] had developed a full statistical analysis on the effect of ECAP route type, die angle, and number of passes on grain size refinement, cryptographic texture, Vickers hardness (HV), and tensile properties of pure Mg. Gu and Toth [53] reported that route A resulted in a structure with a high density of elongated grains, whereas route Bc resulted in ultrafine grained structure with almost recrystallized equiaxed grains [25]. Illgen et al. [54] reported that processing through the odd number of route C resulted in elongated grains, whereas the even number resulted in almost equiaxed grains.

Unfortunately, there are limited studies of the effect of ECAP on pure Mg because of its poor ductility and deformability. Thus, the objective of this study is to investigate the effect of the most important ECAP parameters such as route type and internal channel angle on the microstructural evolution, cryptographic texture, and mechanical properties of pure Mg. To do so, pure Mg was processed using two ECAP dies with channel angles of 90° and 120° through route A, Bc, and C. Scanning electron microscopy (SEM) equipped with electron back-scatter diffraction (EBSD) was used to analyze the microstructure and texture of Mg billets before and after processing. Vickers microhardness and the tensile properties of the pure Mg billets were investigated and correlated with the microstructure findings.

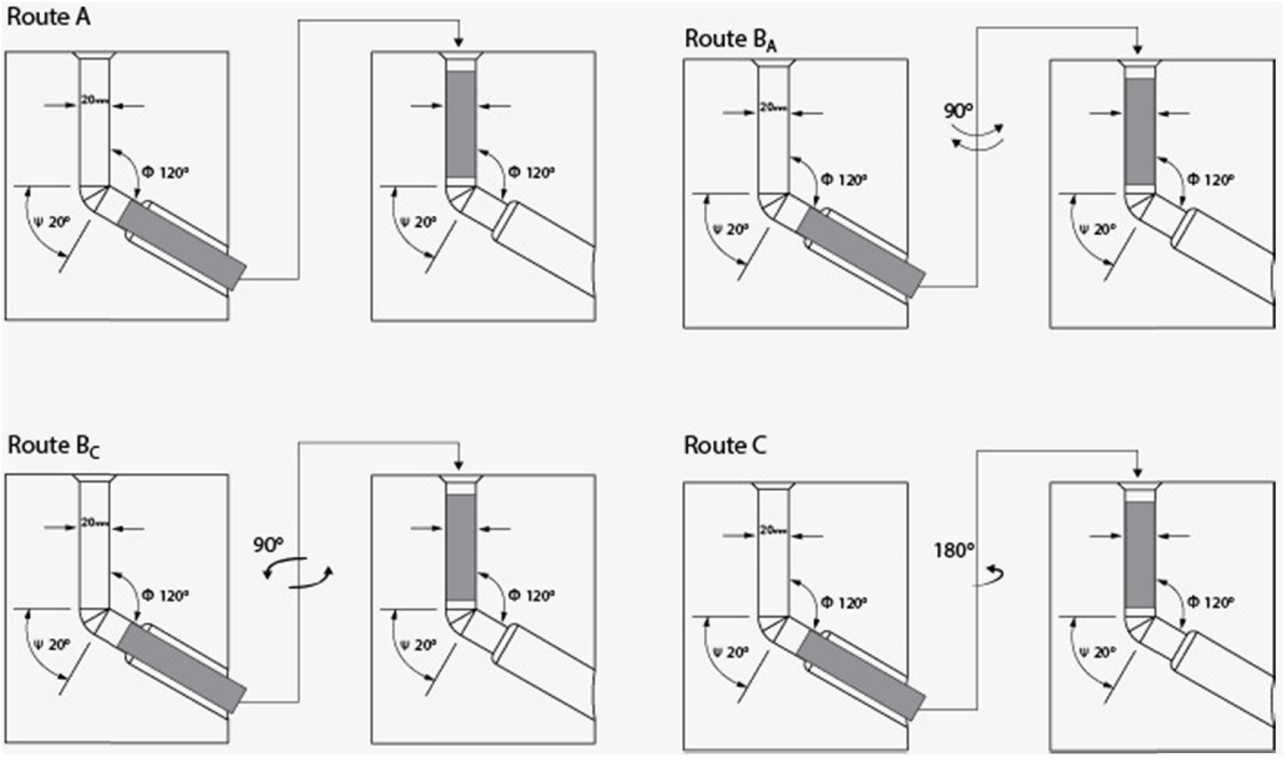

Figure 1: Schematic of the different routes type of ECAP processing.

2 Materials and methods

In this study, the as-received pure Mg rolled billets were 20 mm in diameter and 500 mm in length. A precision-cutting machine was used to section the ECAP samples from the billets, which were 60 mm in length. Before processing, the samples were annealed at 250°C for 1 h and then furnace cooled. Processing via ECAP was performed through 1-pass and 2-passes (2 P) at 225°C through different routes (A, Bc, C) with a 0.05 mm/s ram speed. To decrease the friction between the ECAPed samples and the inner walls of the die, a graphite-based lubricant was applied before each pass. The ECAP die had a fixed outside arc of curvature of angle 20° (Ψ). However, the angle at which the two channels intersected was made a variable. Two internal channel angles ϕ (90° and 120°) were used as shown in Figure 2, and the samples were processed via both of them. The equivalent strain (ε_{eq}) imposed by the die channel based on equation (1) was approximately 0.65 per pass. The equal-channel angular pressed samples were sectioned from the center along their longitudinal section (LS) on the normal plane to the die's entrance and parallel to the flow plane (pressing direction). The reference system axes coincide with the ECAP extrusion direction "*Y*" (ED), the normal direction "*Z*" (ND), and the transversal direction "*X*" (TD).

The microstructural and crystallographic textures of the ECAPed Mg under the different studied conditions were investigated using a field emission scanning electron microscope (FESEM, Hitachi, Ltd, Tokyo, Japan) equipped with a NordlysMax2 EBSD detector. EBSD was performed on the TD-ED plane, top surface, using an SU-70 SEM (Hitachi, Ltd, Tokyo, Japan) operating at a typical current of 1.5 nA and 15 kV. Before EBSD, the sample surfaces were prepared by grinding and mechanical polishing down to 1 µm using a tripod polisher and then chemical polishing with colloidal silica (0.05 µm) for 24 h by a BUEHLER Vibrometer (Buehler, Tucson, AZ, USA).

Hardness was evaluated using a Vickers microhardness testing machine. Samples were loaded for 15 s under a load of 0.5 kg. Tensile properties of Mg ECAPed samples were measured using a universal testing machine (Instron 4210, Norwood, MA, USA). Uniaxial tensile tests were conducted with a strain rate of $10^{-3}\,s^{-1}$ applied at room temperature. Tensile testing was conducted on samples machined according to the E8 M/ASTM standard and sectioned from the central regions of the ECAPed billets. To ensure

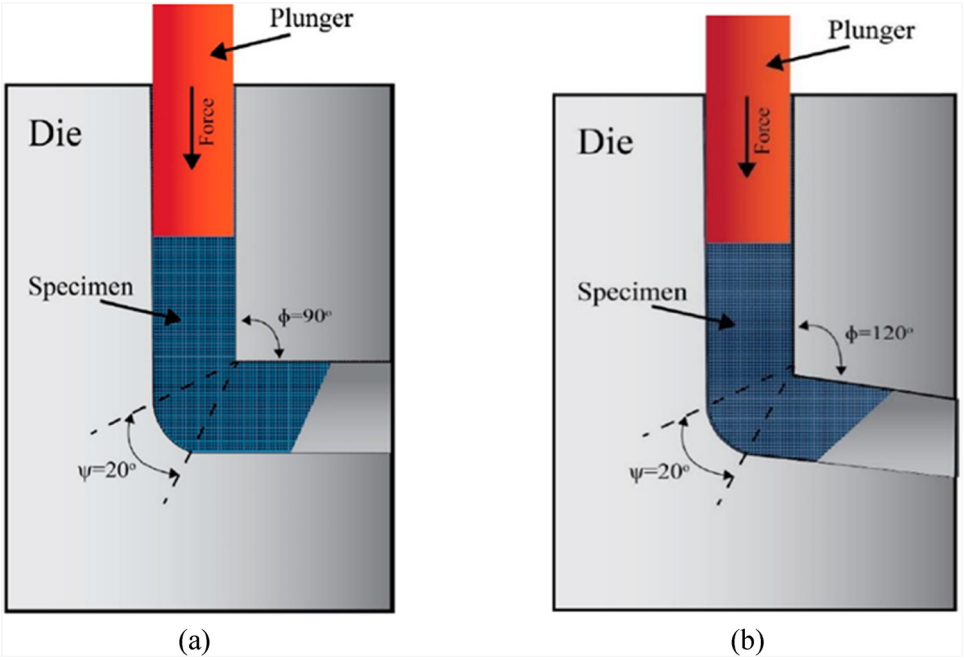

Figure 2: Schematic of the ECAP dies with internal channel angle of (a) 90° and (b) 120°.

the precision of the results, each processing condition was tested using three different samples of that condition.

3 Results and discussion

3.1 Microstructure evolution

The grain structures of the as-annealed pure Mg (AA) and all of the ECAPed samples were investigated using EBSD. The inverse pole figures (IPFs) and their band contrast (BC) maps of the AA billet relative to the ND are exhibited in Figure 3. Low-angle grain boundaries (LAGBs) are characterized by having misorientation angles ranging between 3 and 15°, whereas high-angle grain boundaries (HAGBs) are characterized by having misorientation angles that are greater than 15°. LAGBs are shown in red, and HAGBs are shown in black. A side effect of processing via ECAP is the high friction between the die walls and the processed billets, which consequently increases the density of the HAGBs. In addition, the IPFs and BC maps of the ECAPed billets through the 90° and 120° dies are shown in Figures 4 and 5, respectively. Furthermore, Table 1 lists the relevant grain-size data collected from all Mg samples. From Figure 3a it was clear that the microstructure of AA

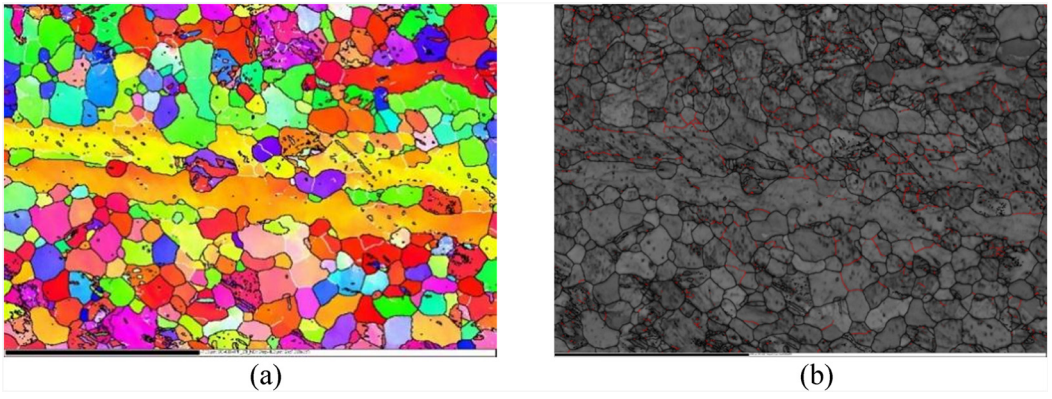

Figure 3: (a) IPF map and (b) BC map with high-angle boundaries >15° in black lines and low-angle boundaries 3–15° in red lines, superimposed for the AA pure Mg.

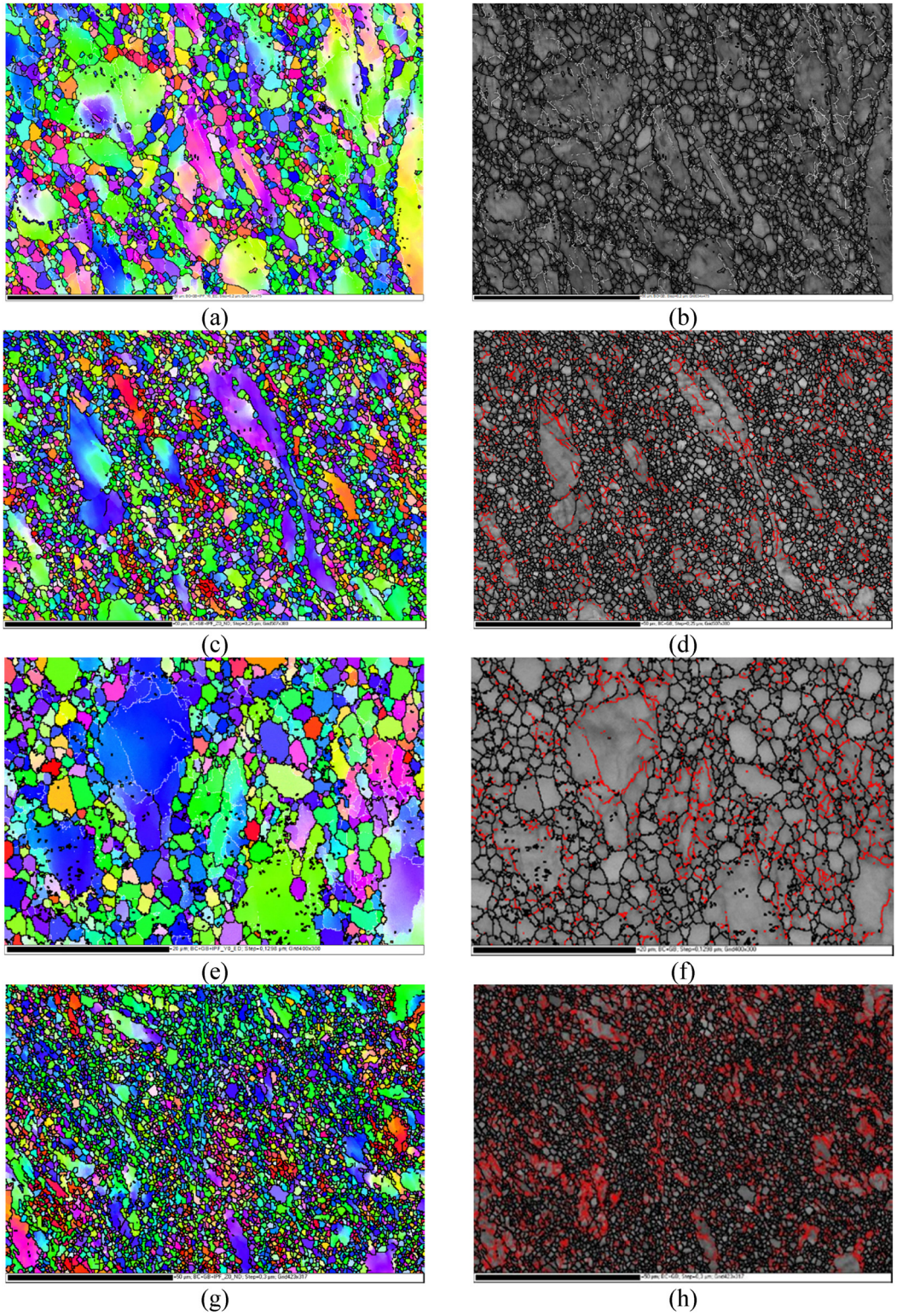

Figure 4: IPF coloring maps and their corresponding band BC maps with high-angle boundaries >15° in black lines and low-angle boundaries 3–15° in white lines (b) and (d, e, h) red lines, superimposed for the Mg billets processed through (a and b) 1-pass or (c and d) 2-passes of route A, (e and f) 2-passes of route Bc, and (g and h) 2-passes of route C using the ECAP die with channel angle of 90°.

Table 1: Grain size data (μm) of all Mg specimens grouped by die angle (ϕ) and route type

Grain size (μm)	AA	ϕ = 90°				ϕ = 120°			
		1-P	2-A	2-Bc	2-C	1-P	2-A	2-Bc	2-C
Minimum	1.106	0.638	0.564	0.507	0.677	1.106	0.677	0.505	0.505
Maximum	34.02	25.454	22.62	9.291	11.052	24.82	24.795	22.727	16.912
Mean grain size	6.338	1.9587	1.692	1.492	1.574	2.62	1.754	1.896	1.94
Standard deviation	5.815	1.515	0.97	0.945	0.667	2.445	1.444	1.433	1.643

primarily revealed a few extra-large grains. In addition, the AA billets revealed equiaxed coarse grains coupled with a few fine grains that were displayed in some limited areas inside the extra-large grains. The minimum and maximum recorded grain size of the AA billets was 1.106 and 34.02 μm, respectively, with the mean grain-size being 6.338 μm. Furthermore, the grain boundaries (GB) map shown in Figure 3b revealed a limited number of LAGBs, which are displayed as red lines.

Processing through 1-pass using the ECAP die with an internal channel angle of 90° (Figure 4a) resulted in a bimodal structure in which heavily deformed and distorted grains were revealed coupled with newly formed fine grains, which indicated that the imposed strain resulted in the dynamic recrystallization process in some areas and formation of the new fine grains, whereas it was not sufficient to refine the grains in other areas. The produced grain size ranged from 0.638 to 25.45 μm, with an average grain size of 1.9587 μm, as listed in Table 1. Furthermore, from Figure 4a it was clear that 1-pass processing resulted in increasing the fraction of LAGBs. The grain size distribution is shown in Figure 6, whereas the misorientation angle distribution is shown in Figure 7 for the Mg billets before and after ECAP processing.

Processing through 2-passes using the 90°-die revealed that the microstructure was dominated by fine grains that were not present in the AA sample before. A few residual large grains remained from the AA sample, but they were heavily deformed. The coarse grains that remained were still equiaxed and homogenously structured. Processing through 2-passes of route A (2-A) revealed increase in areas of fine grains and reduction in areas of coarse grains, as shown in Figure 4c, which was attributed to the increase in the amount of plastic strain through increasing the number of passes. The grain size ranged between 0.564 and 22.62 μm, with an average grain size of 1.692 μm, which indicated that 2-A resulted in decreasing the grain size by 73.3% compared to the AA counterpart. In terms of LAGBs, Figures 4d and 7 revealed that 2 A led to a significant increase in the fraction of LAGBs. In addition, processing through 2-passes of route Bc (2-Bc) resulted in significant refinement (Figure 4e); the grain size ranged between 0.507 and 9.291 μm, and the average grain size was reduced by 76.45% compared to the AA condition. In contrast 2-Bc revealed a significant reduction in the LAGBs (as shown in Figure 4f), which indicated that LAGBs had transferred into HAGBs and an UFG recrystallized structure was attained. Processing through 2-passes of route C (2-C) resulted in significant increases in the areas of recrystallized fine grains, as shown in Figure 4g, and the grain size ranged between 0.677 and 11.052 μm, with average grain size of 1.574 μm, indicating that 2-C reduced the average grain size by 75.1% compared to the AA counterpart. Contrastingly, 2-C revealed a significant increase in the fraction of LAGBs, as shown in Figures 4h and 7. From the aforementioned findings, it was clear that route Bc is the most effective in obtaining UFG equiaxed grains, followed by route C, whereas route A resulted in more elongated grains compared to the others. Furthermore, it can be concluded that route Bc resulted in producing a higher fraction of fine grains, and hence, fine grains with smaller average grain size (as shown in Figure 6 and tabulated in Table 1), followed by route C and finally route A.

To study the effect of ECAP die angle on microstructural evolution, pure Mg billets were processed through 2-passess of different routes. ECAP processing through 1-pass using the 120°-die revealed fewer areas with UFG structure compared to the Mg billets processed using the 90°-die, as shown in Figure 5a. This can be explained by the lower plastic strain of the 120°-die compared to the 90°-die, according to equation (1). Table 1 revealed that 1-pass using the 120°-die resulted in grain size ranging from 1.106 to 24.82 μm, with average grain size of 2.62 μm. In contrast, 1-pass using the 120°-die displayed a higher fraction of LAGBS compared to the 90°-die (Figure 7). Similar to the 90°-die findings, strain accumulation through 2-passes revealed increasing UFG areas and decreasing areas of coarse grains. Processing of 2-A resulted in a bimodal structure, wherein UFG coexisted with elongated coarse grains, as shown in Figure 5c. The grain size ranged between 0.677 and 24.795 μm, with an

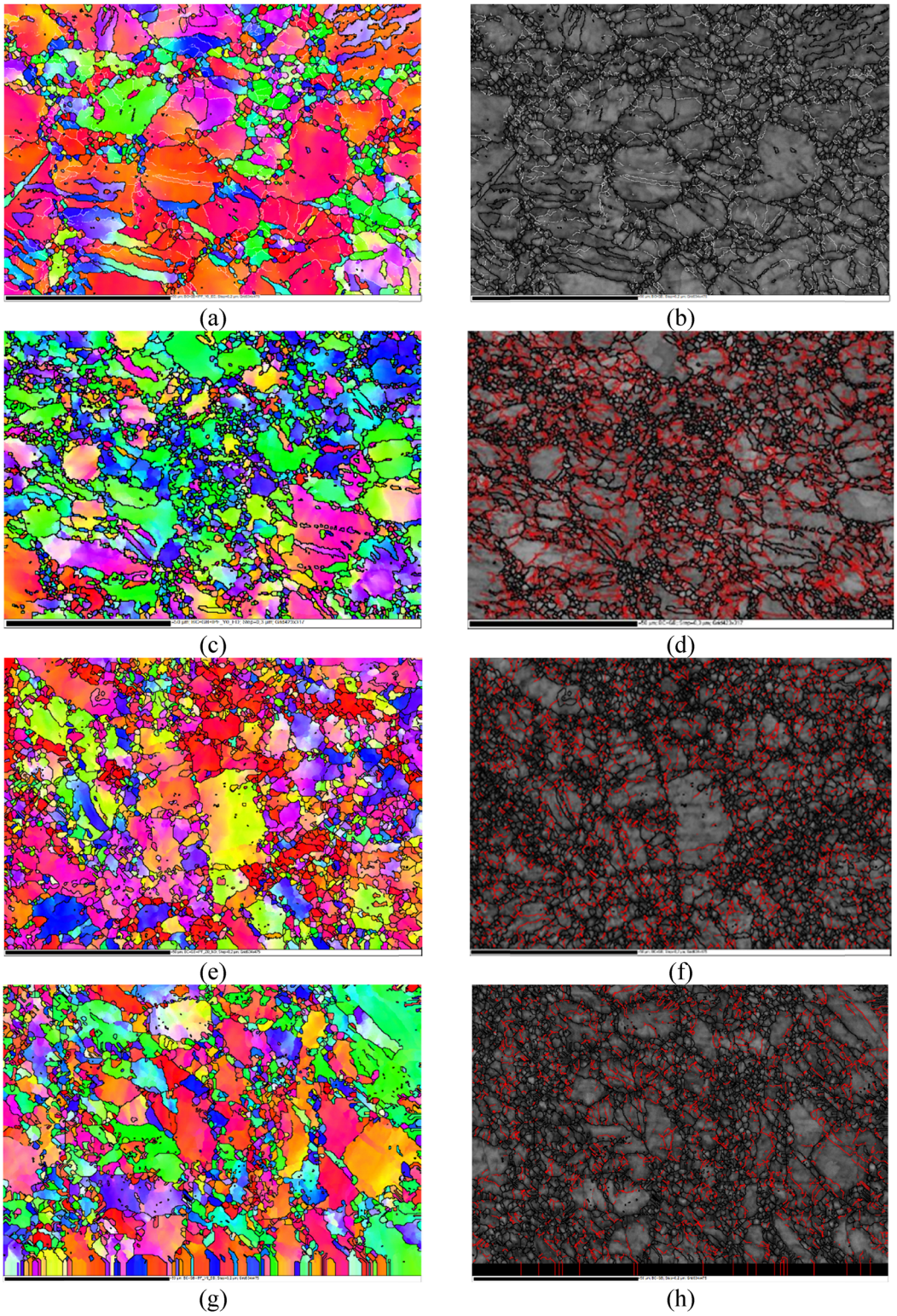

Figure 5: IPF coloring maps and their corresponding band BC maps with high-angle boundaries >15° in black lines and low-angle boundaries 3 –15° in white lines (b) and (d, e, h) red lines, superimposed for the Mg billets processed through (a and b) 1-pass or (c and d) 2-passes of route A, (e and f) 2-passes of route Bc, and (g and h) 2-passes of route C using the ECAP die with channel angle of 120°.

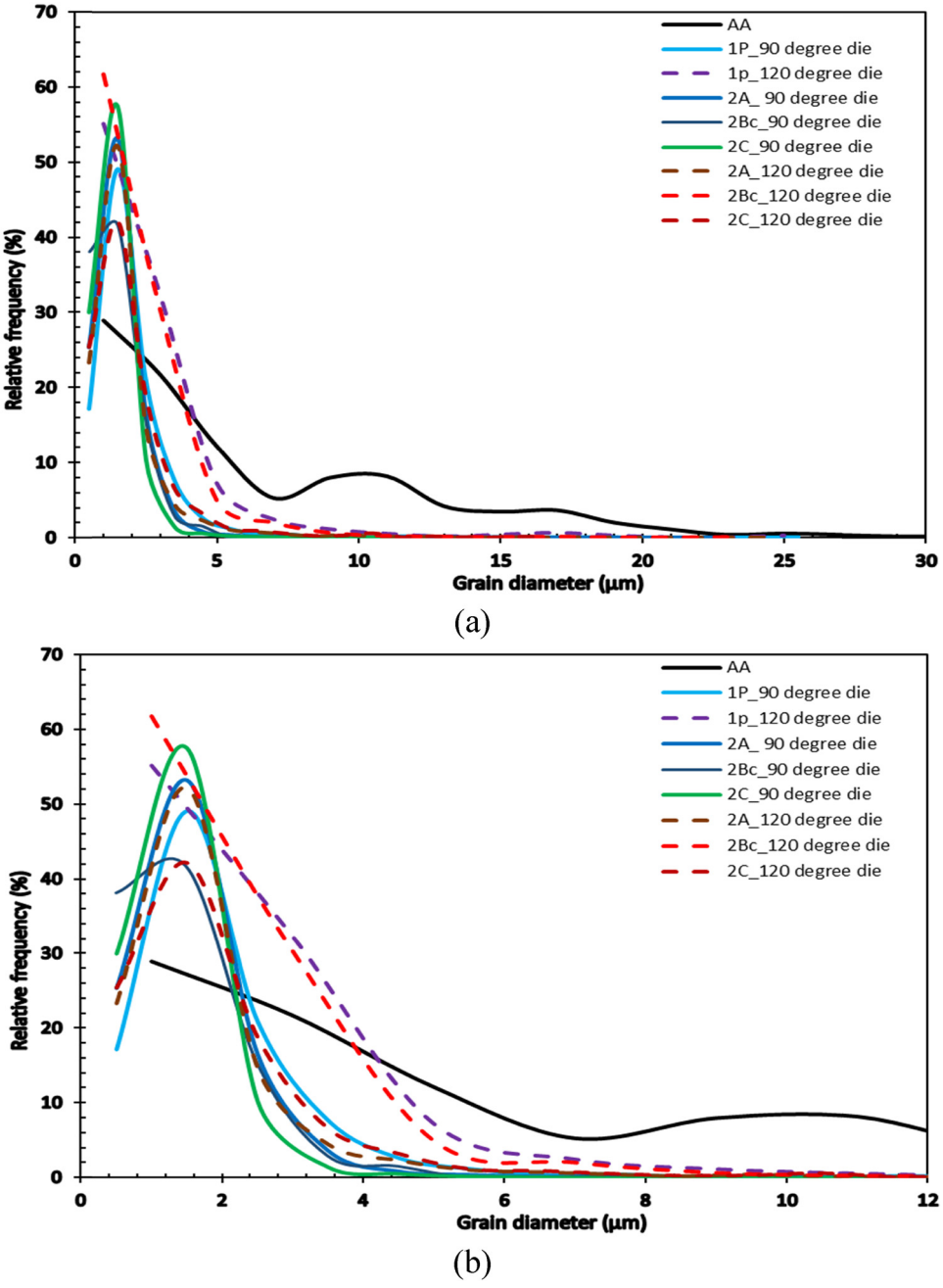

Figure 6: (a) Grain distribution calculated from EBSD data for the AA and ECAPed Mg billets using different die angles of $\phi = 90°$ and $\phi = 120°$ through different route types and (b) magnification of the grain size distribution.

average grain size of 1.754 µm, which indicated that 2-A resulted in refining the grain size to 72.3% compared to the AA counterpart. In addition, 2-A resulted in significant increases in LAGBs, as shown in Figure 5d. Contrastingly, 2-Bc and 2-C resulted in refining the average grain size of pure Mg to 70 and 69.4%, respectively, compared to the AA counterpart. In terms of LAGBs, both 2-Bc and 2-C revealed significant increases in the fraction of the LAGBs compared to the AA condition (Figure 5f and h). Furthermore, from the aforementioned findings, it was clear that for the 120°-die, route A is more effective in grain refining compared to routes Bc and C.

The heterogeneity associated with the AA-Mg microstructure before the ECAP process causes regions to respond differently to the resulting strain. The imposed strain caused dynamic recrystallization to occur in regions with HAGBs and subsequently caused their

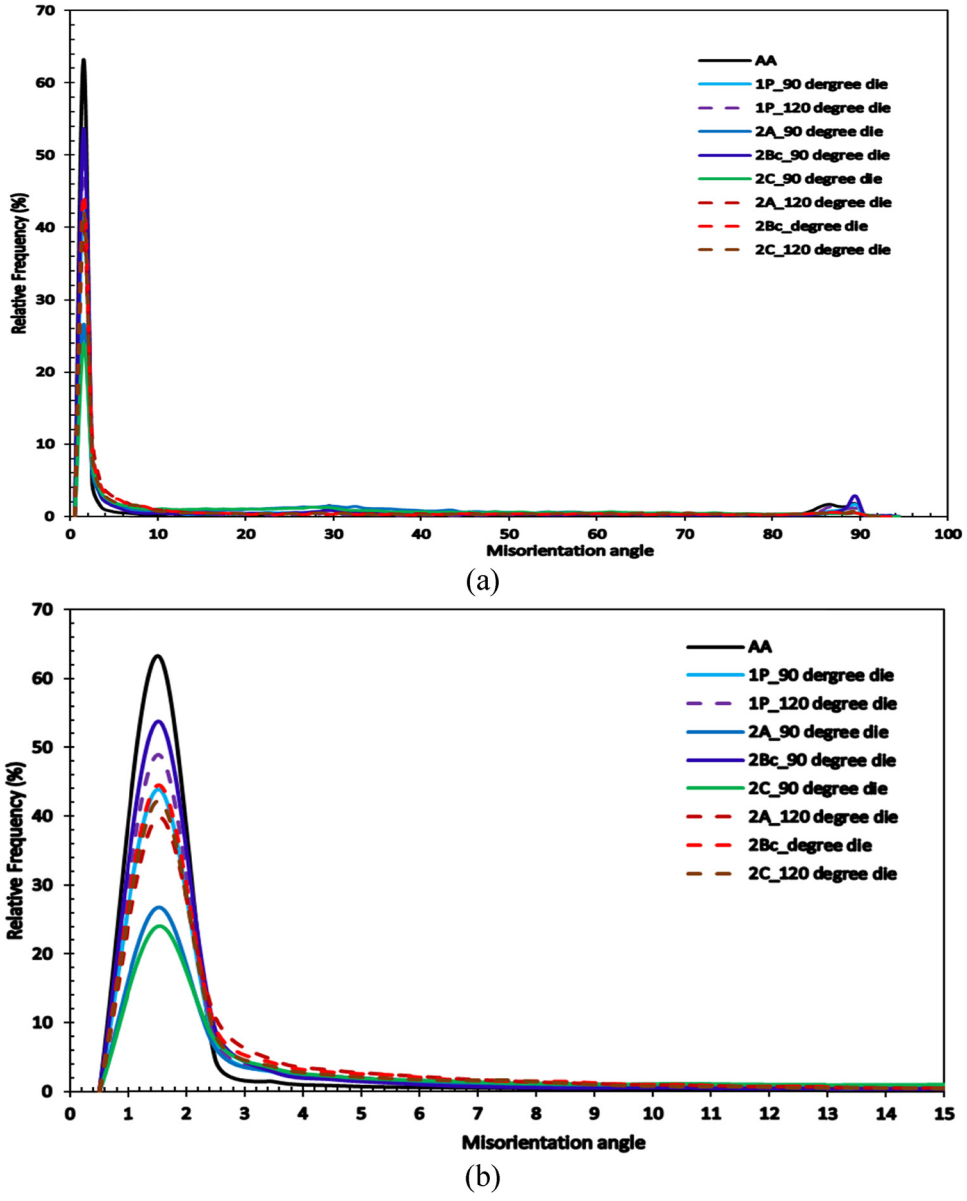

Figure 7: (a) Misorientation angle distribution of the AA and ECAPed billets of pure Mg using different die angles of ϕ = 90° and ϕ = 120° through different route types and (b) magnification of the misorientation angle distribution.

evolution into extremely fine grains. A rapid evolution of the microstructure occurred in routes Bc and C due to the elevated extent of recoverable shearing. However, this sort of evolution was hindered in samples processed by route A due to the repetitive nature of the route, which served only to distort the *Y* plane. For the 90°-die, route Bc revealed transference of a higher fraction of LAGBs into HAGBs (Figure 4f) compared to routes A and C. In contrast, for the 120°-die route A revealed transference of a higher fraction of LAGBs into HAGBs (Figure 5h) compared to routes Bc and C. Accordingly, the higher the transfer of LAGB fractions into HAGBs, the higher the refinement of the grain size and better the strengthening effect, resulting from more resistance to the dislocation motion.

Similar findings were reported in earlier studies. Lei and Zhang [50] reported that 4-passes were enough to refine the pure Mg grain size up to 1.75 µm. Xu et al. [55] reported that processing AZ31 through 4-passes resulted in achieving a homogenous equiaxed microstructure with an average grain size of 7 µm. Alateyah et al. [28] reported that 4 Bc using 90° ECAP die is the most effective ECAP processing condition for ZK30 alloy; 4-Bc, 4-A, and 4-C conditions resulted in refining Mg alloy from 26.69 to 1.94, 2.89, and 2.25 µm, respectively. In addition, Alateyah et al. [22] found that the ECAP die with 90° revealed more

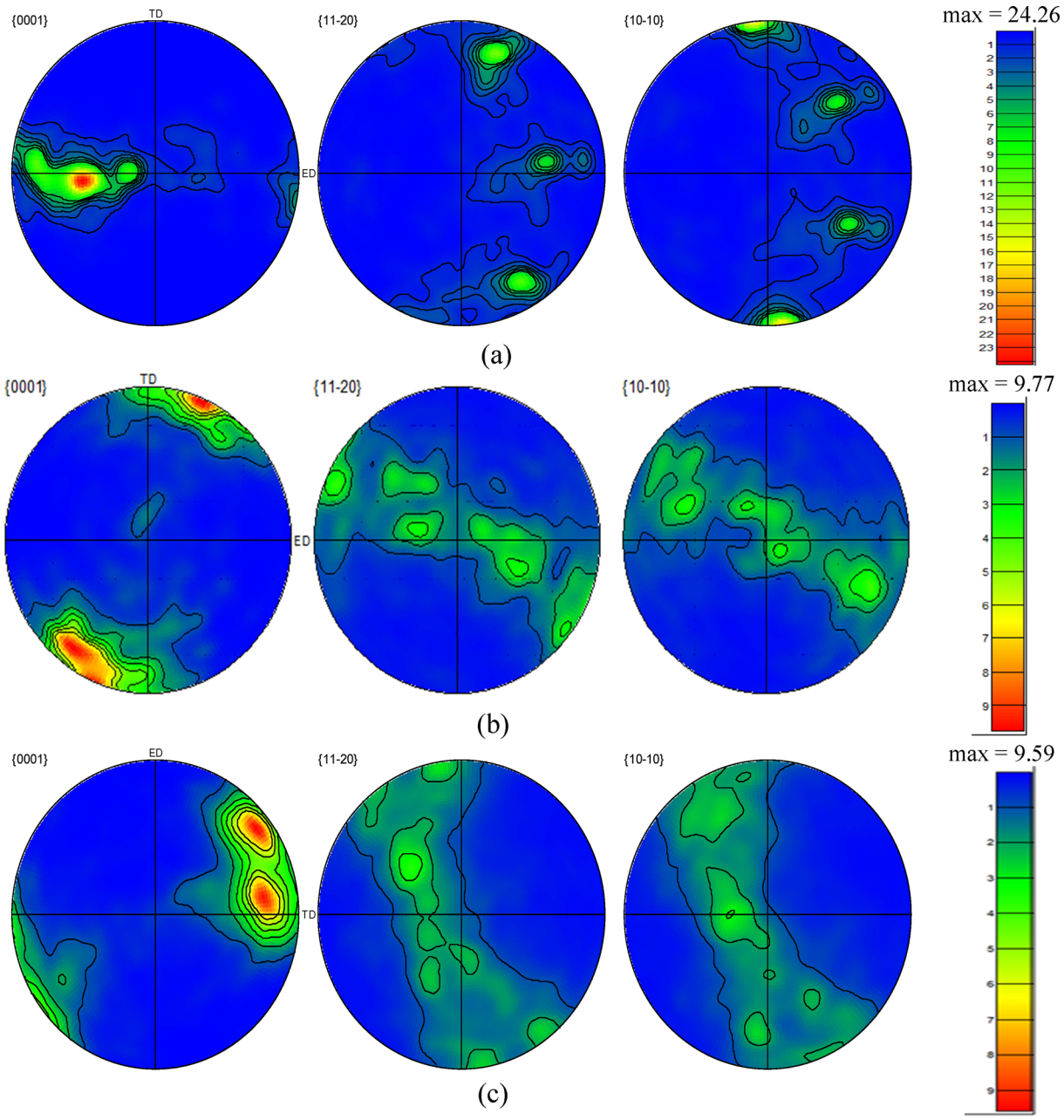

Figure 8: {0001}, {11–20} and {10–10} pole figures of (a) AA-Mg BM and ECAP samples processed using the 90°-die angle processed through (b) 1-pass, (c) 2-A, (d) 2-Bc, and (e) 2-C.

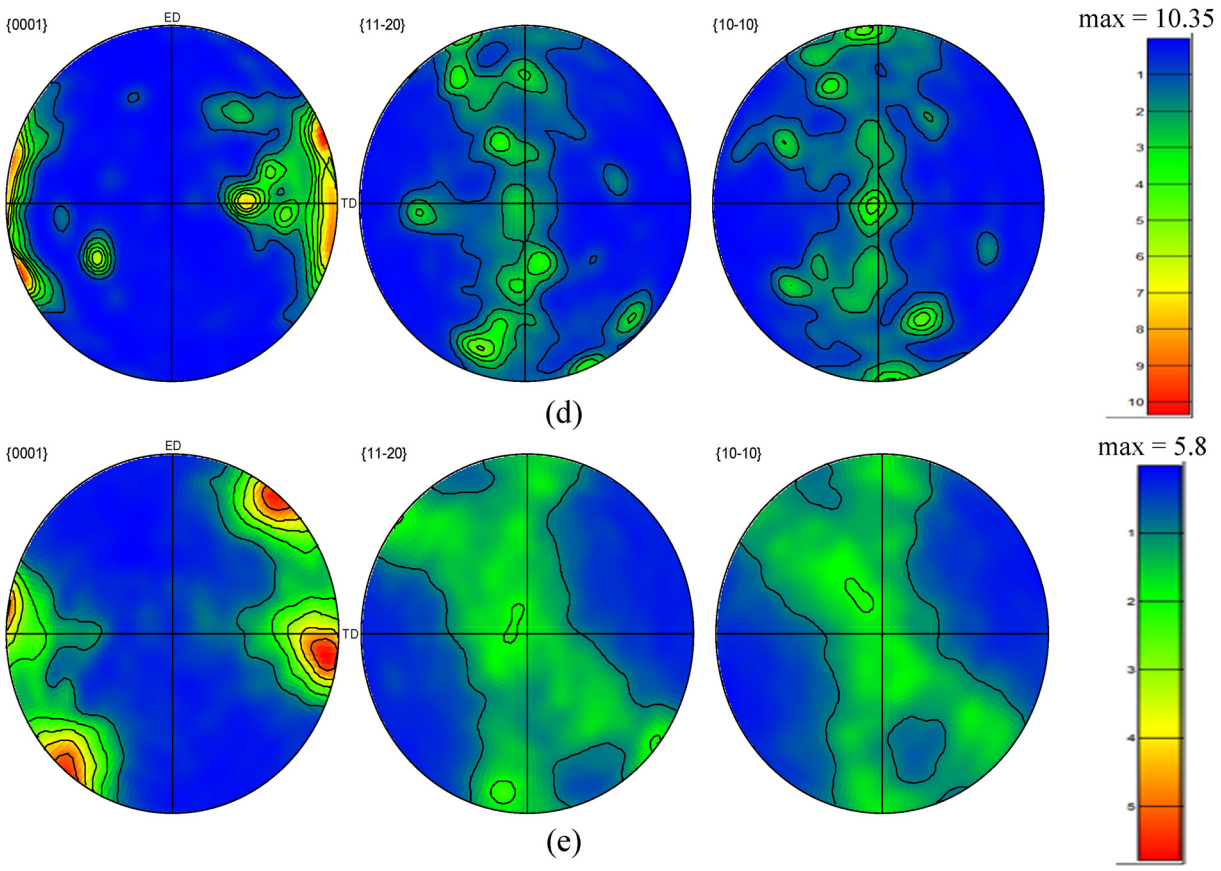

Figure 8: (*Continued*)

efficiency in grain refining of pure Mg, and 4-Bc processing through the ECAP dies with 90° and 120° resulted in reducing the grain size of the AA billets from 6.34 to 0.88 µm and 1.89 µm, respectively. Sankuru et al. [56] reported that 4-passes of all route types led to achieving homogenous equiaxed grains of pure Mg, whereas 4-Bc was the most effective route in grain refinement. Gzyl et al. [57] reported that processing of AZ31B alloy through route A showed less tendency to fracture compared to route Bc and C. Tong et al. [58] reported that route Bc revealed more efficiency in grain refinement of Mg–Zn–Ca alloy, followed by route C and finally route A. In addition, they explained the reduction in LAGBs during the multiple passes by the transferring into HAGBs.

3.2 Crystallographic texture

Figure 8 shows the pole figures of Mg billets before and after processing using the 90°-die. Similar pole figures of the 120°-die are shown in Figure 9. The poles are plotted for three families of planes: {0001}, {10–10}, and {11–20}. From Figure 8a, the texture of the AA billets seems to possess strong texture components with a max intensity of 24.26 times random, with the densest collection of {0001} poles occurring on the same horizontal line as the extrusion direction (ED). During plastic deformation of HCP metals, the ideal shear texture is predominately dependent on the active slip systems. HCP crystals have fewer slip systems than the FCC and BCC crystal structures, being restricted to only the basal {0001} <11–20>, pyramidal {10–11} <11–20>, or prismatic {10–10} <11–20> slip systems [59,60]. After ECAP processing, the predominant texture was that of simple shear with the shear plane at a 45° angle with the ED, which indicates that the basal slip system became active with ECAP processing.

Processing through 1-pass using the 90°-die resulted in rotating the {0001} basal planes by about 45° around the normal direction as shown in Figure 8b, which is aligned with the shear plane normal (SPN), which can be attributed to the basal slip activation during the first ECAP pass [22]. Furthermore, 1-pass resulted in reducing the max intensity of the texture from 24.26 times random for the AA billets to 9.77 times random, which can be

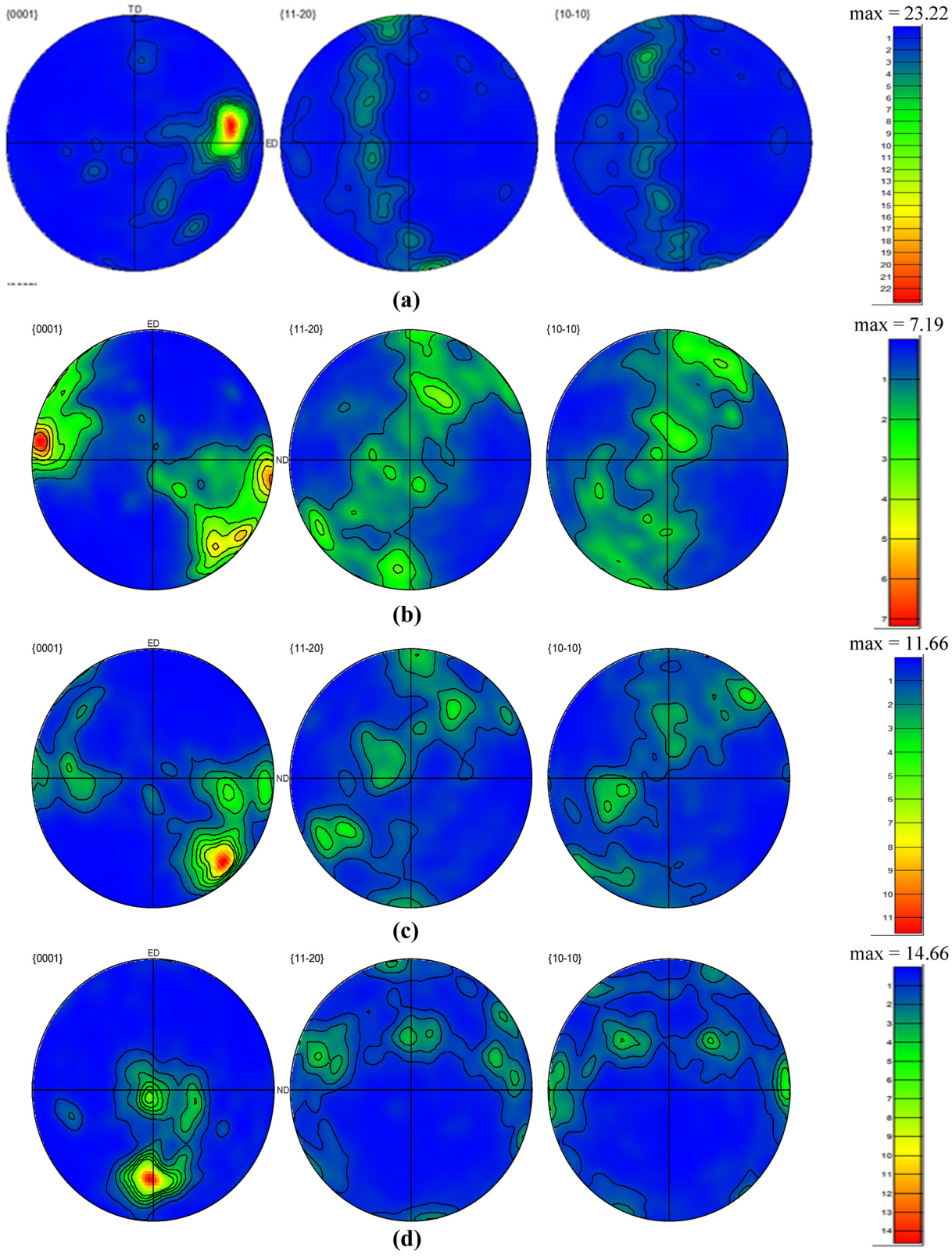

Figure 9: {0001}, {11–20} and {10–10} pole figures of the ECAP samples processed using the 120° die angle processed through (a) 1-pass, (b) 2-A, (c) 2-Bc, and (d) 2-C.

attributed to the few numbers of active slip systems after 1-pass processing and agreed with ref. [55]. The crystallographic texture of the ECAP processed samples was found to be weaker across all die angles and routes used for 2-passes processing, which negatively affects the strength. Figure 8 shows the texture strength of the samples processes using the 90°-die. The weakest texture was recorded in the sample processed via route C, with a maximum texture intensity of 5.8 times random. The samples processed via routes A and Bc with the same die angle showed slightly stronger texture intensities of 9.59 and 10.35 times random, respectively.

The samples processed with die angle 120° showed slightly stronger texture components, as shown in Figure 9. Figure 9a shows that 1-pass processing using the 120°-die led to a strong texture; the max recorded intensity was 23.22 times random. The {0001} basal planes were oriented parallel to the ED. Furthermore, 2-passes of the different routes resulted in a much weaker texture, as shown in Figure 9. The strongest texture component occurred in route C, which was 14.66 times random, whereas those of routes A and Bc were 7.19 and 11.66 times random, respectively. It can be argued that the shear plane positions change in the second pass, which results in the SPN alignment with the shear direction (SD) and TD with the ED. However, using route A resulted in strong basal poles that rotate around the TD axis by 130°, which agreed with that reported by Gautam and Biswas [61].

The texture components seem to have rotated significantly away from their ideal position. This can be attributed to the rotation of SD and SPN relative to the die angle as a consequence of the 120°-die angle. The intense {0001} poles were tilted with respect to the ED with various angles depending on the route used. As previously stated, all processed texture components were of lower intensity and strength, compared to the AA condition, which becomes evident by looking at the {0001} pole figures (Figures 8 and 9). This decline in intensity can be argued to represent the slip system activation. Indeed, the rotation of the basal plane during ECAP processing can be explained by the shearing stresses parallel to the basal planes [55]. In addition, the crystallographic texture findings of pure Mg perfectly matched with earlier studies for pure Mg [22,62], AZ31B Mg alloy [63], ZK30 alloy [27,28], and AZ31 alloy [64].

3.3 Mechanical properties

HV values were measured for the AA and ECAP processed samples through different ϕ (90° and 120°) and as a function of the three different routes (A, Bc, C). The HV values are illustrated in Table 2. The average HV value of the AA sample was 26. Inspection of Table 2 shows that hardness increased considerably after ECAP processing. Moreover, the 90°-die consistently produced higher hardness values than the corresponding ϕ = 120°-die across all routes. ECAP processing through 1-pass using the 90°-die and 120°-die resulted in increasing the HV value by 61.5 and 50%, respectively, compared to the AA counterpart. In addition, 2-A, 2-Bc, and 2-C processing through the 90°-die displayed additional increases in the HV values of 76.9, 96, and 84.6%, respectively, compared to the AA counterpart. Furthermore, 2-A, 2-Bc, and 2-C processing through the 90°-die experienced an additional increase in the HV values by 9.5, 8.5, and 9%, respectively, in comparison with the samples processed through 2-A, 2-Bc, and 2-C using the 120°-die.

Accordingly, the HV findings were matched with the microstructural evolution shown in Figures 4 and 5. In addition, the significant improvement in the HV values evolved as a result of the underlying grain refinement, route Bc possessed the lowest grain size. Consequently, the decrease in hardness with increasing ϕ can be explained by the lower plastic strain imposed on the samples at higher angles.

Tensile tests were conducted on the AA and ECAPed Mg billets at room temperature. The stress–strain curves

Table 2: Mechanical properties of the AA and ECAPed samples using different die angles, ϕ of 90° and 120°, and different route types, A, Bc, and C

Grain size (μm)	AA	ϕ = 90°				ϕ = 120°			
		1-P	2-A	2-Bc	2-C	1-P	2-A	2-Bc	2-C
Hardness (HV)	26	42	46	51	48	39	42	47	44
σ_u (MPa)	224	295	278	310	322	268	262	274	260
Ductility (%)	0.21	0.37	0.38	0.365	0.31	0.33	0.4	0.37	0.38

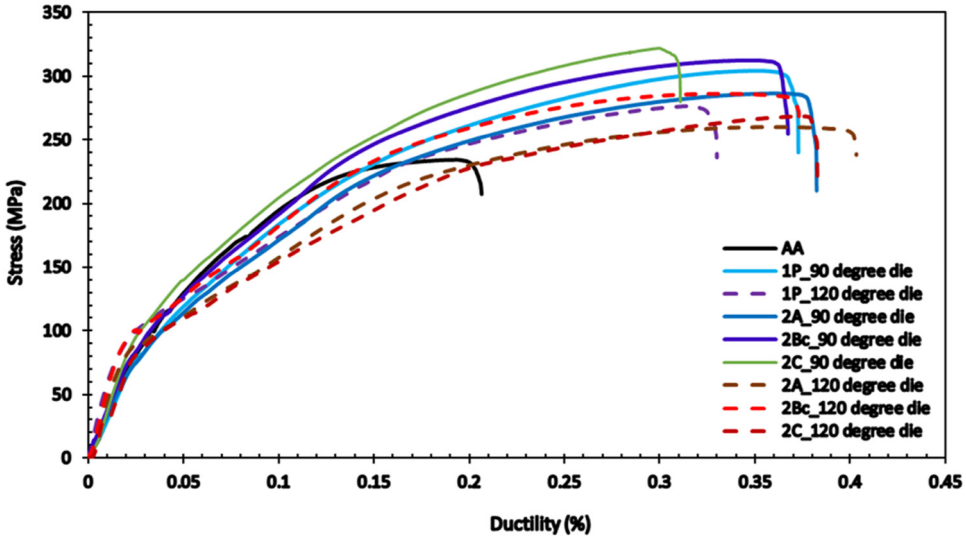

Figure 10: Tensile stress–strain curves of Mg billets processed through ECAP using the 90°-die and 120°-die via different numbers of passes and route types.

extracted from the tensile tests are shown in Figure 10. From Figure 10, it is clear that neither the ECAP die angle nor the route type had a significant effect on the yield strength, and all the processing conditions displayed insignificant change in the yield strength. The ultimate tensile strength (σ_u) and the ductility Mg at fracture are listed in Table 2. Table 2 clearly shows that both σ_u and Mg ductility significantly improved after processing. For the ECAP die with channel angle of 90°, 1-pass increased σ_u by 31.7%, coupled with improving the ductility by 76%, whereas 1-pass using the 120°-die resulted in increasing the σ_u by 19.6%, coupled with improving the ductility by 57%, compared to the AA counterpart. ECAP processing through the 90°-die led to improving σ_u by 14.1, 38.4, and 43.75%, coupled with improving the Mg ductility by 80.9, 73.5, and 47.6%, through processing via 2-A, 2-Bc, and 2-C, respectively, compared to the AA counterpart. In comparison with the sample processed through 2-A, 2-Bc, and 2-C using ECAP die with 120°, their counterparts processed using the 90°-die revealed notable improvements in σ_u by 6.1, 13.14, and 23.8%, respectively, whereas the ductility was reduced by 5.26, 1.35 and 18.4%, respectively. Accordingly, the 120°-die samples consistently had higher ductility values than those of the corresponding 90°-die across all routes, which is a result of the reduced strain applied. The increase in σ_u with both 90°- and 120°-dies can be attributed to the ultrafine grains produced from processing. In addition, the 90°-die revealed higher σ_u compared to the 120°-die counterpart due to the higher plastic strain of the 90°-die compared to the 120°-die, according to equation (1), which resulted in higher grain refinement, as shown in Figures 4 and 5 and as listed in Table 1. Similar findings were reported earlier for pure Mg [22,26] and ZK30 [24,27,28]. Furthermore, the reduction in the ductility in 90° billets during processing through multiple passes of different route types could be assigned to the smaller grain size compared to the 120°-die, as a result of material strengthening, leading to ductility reduction [22]. According to Hughes' theoretical model, the imposed strain results in dislocation movement [65]. The dislocations are then absorbed by the LAGBs, which consequently gradually transform into stable HAGBs. ECAP also results in the creation of new dislocations, subsequently increasing the dislocation density, which negatively affects the dislocations' ability to move [66]. Thus, the hardness and ultimate tensile strength of AA-Mg are enhanced after the ECAP process. Finally, grain refinement caused grain-boundary strengthening of the samples [67].

4 Conclusion

Pure Mg billets were processed through two ECAP dies with internal channel angle of 90° and 120° through up to 2-passes of routes A, Bc, and C at 225°C. Microstructural evolution, crystallographic texture, and mechanical properties of the Mg billets were investigated to study the effect of ECAP die angle and route type on the plastic strain homogeneity. The following conclusions can be drawn:

1. The 90°-die is more capable of grain refinement than the 120°-die.

2. Route Bc is the most effective in grain refinement compared to other routes.
3. Processing via 2-Bc using the 90°-die experienced a homogenous distribution of UFG with a reduced average grain size of 74.45% compared to the AA counterpart.
4. Processing of 2-C using the 120°-die displayed the strongest texture compared with the other processing conditions with a texture intensity of 14.66 times random.
5. Processing of 2-Bc using the 90°-die revealed an increase in the HV of 96% compared to the AA counterpart.
6. The 90°-die revealed higher tensile strength compared to the 120°-die.
7. Processing of 2-A, 2-Bc, and 2-C through the 90°-die led to improved tensile strength by 14.1, 38.4 and 43.75%, respectively, compared to the AA counterpart.

Acknowledgements: The researcher would like to thank the Deanship of Scientific Research, Qassim University, for funding the publication of this project.

Funding information: This research received no external funding.

Conflict of interest: The authors declare no conflict of interest.

Institutional review board statement: Not applicable.

Informed consent statement: Not applicable.

Data availability statement: All raw data supporting the conclusions of this paper were provided by the author.

References

[1] Mostaed E, Vedani M, Hashempour M, Bestetti M. Influence of ECAP process on mechanical and corrosion properties of pure Mg and ZK60 magnesium alloy for biodegradable stent applications. Biomatter. 2014;4:28283.
[2] Amani S, Faraji G. Recrystallization and mechanical properties of WE43 magnesium alloy processed via cyclic expansion extrusion. Int J Miner Metall Mater. 2018;25(6):672–81.
[3] Witte F. The history of biodegradable magnesium implants: A review. Acta Biomater. 2010 May 1;6(5):1680–92.
[4] Mordike BL, Ebert T. Magnesium properties - applications - potential. Mater Sci Eng A. 2001;302(1):37–45.
[5] Shapiro AE. Magnesium and magnesium alloys. In: AWS, editor. Aws Brazing Handbook. 5th edn; 2007. p. 106–18.
[6] Kainer KU, Mordike BL. Magnesium alloys and their applications. Weinheim: Wiley-Vch; 2000.
[7] Kojima Y. Platform science and technology for advanced magnesium alloys. Mater Sci Forum. 2000;350–351:3–18.
[8] Kuwahara H, Al-Abdullat Y, Ohta M, Tsutsumi S, Ikeuchi K, Mazaki N, et al. Surface reaction of magnesium in Hank's solutions. Mater Sci Forum. 2000;350–351:349–58.
[9] Gupta M, Sharon NML. Magnesium, magnesium alloys, and magnesium composites. NY, USA: Wiley; 2011. p. 39–85.
[10] Kim JJ, Do SH. Recent development and applications of magnesium alloys in the Hyundai and Kia Motors Corporation. Mater Trans. 2008;49(5):894–7.
[11] Agnew SR, Duygulu Ö. Plastic anisotropy and the role of non-basal slip in magnesium alloy AZ31B. Int J Plast. 2005;21(6):1161–93.
[12] Chulist R, Czaja P, Tokarski T, Kuksgauzen I, Chumlyakov YI. Orthogonal shear process in Ni-Mn-Sn single crystal. Int J Plast. 2019 Mar 1;114:63–71.
[13] Sułkowski B, Chulist R. Twin-induced stability and mechanical properties of pure magnesium. Mater Sci Eng A. 2019;749:89–95.
[14] Agnew SR. Deformation mechanisms of magnesium alloys. Advances in wrought magnesium alloys. Sawston, UK: Woodhead Publishing, Elsevier; 2012. p. 63–104.
[15] Hadadzadeh A, Wells MA. Analysis of the hot deformation of ZK60 magnesium alloy. J Magnes Alloy. 2017;5(4):369–87.
[16] Rao KP, Prasad YVRK, Dzwonczyk J, Hort N, Kainer KU. Hot deformation mechanisms in AZ31 magnesium alloy extruded at different temperatures: Impact of texture. Metals. 2012;2(3):292–312.
[17] Al-Samman T, Molodov KD, Molodov DA, Gottstein G, Suwas S. Softening and dynamic recrystallization in magnesium single crystals during *c*-axis compression. Acta Mater. 2012 Jan 1;60(2):537–45.
[18] Wang HY, Yu ZP, Zhang L, Liu CG, Zha M, Wang C, et al. Achieving high strength and high ductility in magnesium alloy using hard-plate rolling (HPR) process. Sci Rep. 2015 Nov 25;5(1):1–9.
[19] Xu W, Birbilis N, Sha G, Wang Y, Daniels JE, Xiao Y, et al. A high-specific-strength and corrosion-resistant magnesium alloy. Nat Mater. 2015;14(12):1229–35.
[20] Alateyah AI, Aljohani TA, Alawad MO, Elkatatny S, El-Garaihy WH. Improving the corrosion behavior of biodegradable AM60 alloy through plasma electrolytic oxidation. Metals. 2021 Jun 11;11(6):953.
[21] Wang LP, Chen T, Jiang WY, Feng YC, Cao GJ, Zhu Y. Microstructure and mechanical properties of AM60B magnesium alloy prepared by cyclic extrusion compression. Trans Nonferrous Met Soc China. 2013 Nov 1;23(11):3200–5.
[22] Alateyah AI, Ahmed MMZ, Alawad MO, Elkatatny S, Zedan Y, Nassef A, et al. Effect of ECAP die angle on the strain homogeneity, microstructural evolution, crystallographic texture and mechanical properties of pure magnesium: Numerical simulation and experimental approach. J Mater Res Technol. 2022 Mar 1;17:1491–511.
[23] Almenaif O, Alhumaydani Y, Alnafisah M, Aldhalaan M, Alateyah AI, El-Garaihy WH. A computational investigation into the effect of equal channel angular processing on the mechanical properties of severely deformed ZK60 alloy

validated by experiments. Am J Eng Appl Sci. 2020 Jun 9;13(2):296–310.
[24] El-Garaihy WH, Alateyah AI, Alawad MO, Aljohani TA. Improving the corrosion behavior and mechanical properties of biodegradable Mg–Zn–Zr alloys through ecap for usage in biomedical applications. Miner Met Mater Ser. 2022;259–69.
[25] Alateyah AI, Aljohani TA, Alawad MO, El-Hafez HA, Almutairi AN, Alharbi ES, et al. Improved corrosion behavior of AZ31 alloy through ECAP processing. Metals. 2021 Feb 21;11(2):363.
[26] Alateyah AI, El-Garaihy WH, Alawad MO, Sanabary S, el Elkatatny S, Dahish HA, et al. The effect of ECAP processing conditions on microstructural evolution and mechanical properties of pure magnesium—experimental, mathematical empirical and response surface approach. Materials. 2022 Aug 1;15:15.
[27] Alateyah AI, Alawad MO, Aljohani TA, El-Garaihy WH. Influence of ultrafine-grained microstructure and texture evolution of ECAPed ZK30 magnesium alloy on the corrosion behavior in different corrosive agents. Materials. 2022;15(16):5515.
[28] Alateyah AI, Alawad MO, Aljohani TA, El-Garaihy WH. Effect of ECAP route type on the microstructural evolution, crystallographic texture, electrochemical behavior and mechanical properties of ZK30 biodegradable magnesium alloy. Materials. 2022 Sep 2;15(17):6088.
[29] She J, Peng P, Tang AT, Zhang JY, Mao JJ, Liu TT, et al. Novel online twist extrusion process for bulk magnesium alloys. Mater Des. 2019 Nov 15;182:108011.
[30] Yang Z, Ma A, Xu B, Jiang J, Sun J. Corrosion behavior of AZ91 Mg alloy with a heterogeneous structure produced by ECAP. Corros Sci. 2021 Jul 15;187:109517.
[31] Alateyah AI, Ahmed MMZ, Zedan Y, El-Hafez HA, Alawad MO, El-Garaihy WH. Experimental and numerical investigation of the ECAP processed copper: Microstructural evolution, crystallographic texture and hardness homogeneity. Metals. 2021 Apr 9;11(4):607.
[32] Valiev RZ, Langdon TG. Principles of equal-channel angular pressing as a processing tool for grain refinement. Prog Mater Sci. 2006 Sep 1;51(7):881–981.
[33] Alateyah AI, Alharbi M, El-Hafez HA, El-Garaihy WH. The effect of equal-channel angular pressing processing on microstructural evolution, hardness homogeneity, and mechanical properties of pure aluminum. SAE Int J Mater Manuf. 2020 Jul 25;14(2):113–25.
[34] El-Shenawy M, Ahmed MMZ, Nassef A, El-Hadek M, Alzahrani B, Zedan Y, et al. Effect of ECAP on the plastic strain homogeneity, microstructural evolution, crystallographic texture and mechanical properties of AA2xxx aluminum alloy. Met 2021. 2021 Jun 9;11(6):938.
[35] El-Garaihy WH, Fouad DM, Salem HG. Multi-channel Spiral Twist Extrusion (MCSTE): A novel severe plastic deformation technique for grain refinement. Metall Mater Trans A Phys Metall Mater Sci. 2018 Jul 1;49(7):2854–64.
[36] Fouad DM, Moataz A, El-Garaihy WH, Salem HG. Numerical and experimental analysis of multi-channel spiral twist extrusion processing of AA5083. Mater Sci Eng A. 2019;764:138216.
[37] Fouad DM, El-Garaihy WH, Ahmed MMZ, El-Sayed Seleman MM, Salem HG. Influence of multi-channel spiral twist extrusion (MCSTE) processing on structural evolution, crystallographic texture and mechanical properties of AA1100. Mater Sci Eng A. 2018 Nov 8;737:166–75.
[38] Fouad DM, El-Garaihy WH, Ahmed MMZ, Albaijan I, El-Sayed Seleman MM, Salem HG. Grain structure evolution and mechanical properties of multi-channel spiral twist extruded AA5083. Metals. 2021;11(8):1276.
[39] Ghazanlou SI, Eghbali B, Petrov R. Microstructural evolution and strengthening mechanisms in Al7075/graphene nanoplates/carbon nano-tubes composite processed through accumulative roll bonding. Mater Sci Eng A. 2021 Mar 11;807:140877.
[40] Kong Y, Pu Q, Jia Z, Liu M, Roven HJ, Jia J, et al. Microstructure and property evolution of Al-0.4Fe-0.15Zr-0.25Er alloy processed by high pressure torsion. J Alloy Compd. 2020 May 25;824:153949.
[41] Bednarczyk W, Kawałko J, Wątroba M, Gao N, Starink MJ, Bała P, et al. Microstructure and mechanical properties of a Zn-0.5Cu alloy processed by high-pressure torsion. Mater Sci Eng A. 2020;776:139047
[42] El-Garaihy W, Rassoul E. Forum HSMS, 2014 undefined. Forum HSMS, 2014 undefined. Consolidation of high performance AA6061 and AA6061-SiCp composite processed by high pressure torsion. Trans Tech Publ. 2014;783–786:2623–8.
[43] El-Garaihy W, el Rassoul ESA, Ateyah AA, Alaskari AM, Oraby S. Data manipulation approach and parameters interrelationships of the high-pressure torsion for AA6061-15% SiCp composite. SAE Int J Mater Manuf. 2018;11(3):167–82.
[44] Salem HG, El-Garaihy WH, Rassoul ESMA. Influence of high pressure torsion on the consolidation behavior and mechanical properties of AA6061-SiCP composites powders. TMS Annu Meet. 2012;1:553–60.
[45] Shuai GL, Li Z, Zhang DT, Tong YX, Li L. The mechanical property and electrical conductivity evolution of Al–Fe alloy between room temperature and elevated temperature ECAP. Vacuum. 2021;183(2):109813.
[46] Segal VM. Materials processing by simple shear. Mater Sci Eng A. 1995 Jul 1;197(2):157–64.
[47] Alawadhi MY, Sabbaghianrad S, Huang Y, Langdon TG. Evaluating the paradox of strength and ductility in ultrafine-grained oxygen-free copper processed by ECAP at room temperature. Mater Sci Eng A. 2021;802:140546.
[48] Iwahashi Y, Wang J, Horita Z, Nemoto M, Langdon TG. Principle of equal-channel angular pressing for the processing of ultra-fine grained materials. Scr Mater. 1996 Jul 15;35(2):143–6.
[49] Naik GM, Narendranath S, Kumar SS. Effect of ECAP die angles on microstructure mechanical properties and corrosion behavior of AZ80 Mg alloy. J Mater Eng Perform. 2019;28(5):2610–9.
[50] Lei W, Zhang H. Analysis of microstructural evolution and compressive properties for pure Mg after room-temperature ECAP. Mater Lett. 2020;271:127781.
[51] Shaeri MH, Salehi MT, Seyyedein SH, Abutalebi MR, Park JK. Characterization of microstructure and deformation texture during equal channel angular pressing of Al–Zn–Mg–Cu alloy. J Alloys Compd. 2013;576:350–7.
[52] Venkatachalam P, Kumar SR, Ravisankar B, Paul VT, Vijayalakshmi M. Effect of processing routes on microstructure and mechanical properties of 2014 Al alloy processed by equal channel angular pressing. Trans Nonferrous Met Soc China. 2010;20(10):1822–8.

[53] Gu CF, Tóth LS. The origin of strain reversal texture in equal channel angular pressing. Acta Mater. 2011 Aug;59(14):5749–57.
[54] Illgen C, Frint P, Gruber M, Volk W, Wagner MFX. Evolution of grain refinement in AA5083 sheet metal processed by ECAP. Miner Met Mater Ser. 2020;362–9.
[55] Xu B, Xiao L, Zhou H, Sun J, Yang Z, Han J, et al. Microstructure and anisotropic mechanical behavior of the high-strength and ductility AZ91 Mg alloy processed by hot extrusion and multi-pass RD-ECAP. Mater Sci Eng A. 2020;780:139191.
[56] Sankuru AB, Sunkara H, Sethuraman S, Gudimetla K, Ravisankar B, Kumaresh, et al. Effect of processing route on microstructure, mechanical and dry sliding wear behavior of commercially pure magnesium processed by ECAP with back pressure. Trans Indian Inst Met. 2021 Nov 1;74(11):2659–69.
[57] Gzyl M, Rosochowski A, Boczkal S, Qarni MJ. The origin of fracture in the I-ECAP of AZ31B magnesium alloy. Metall Mater Trans A Phys Metall Mater Sci. 2015 Nov 1;46(11):5275–84.
[58] Tong LB, Zheng MY, Hu XS, Wu K, Xu SW, Kamado S, et al. Influence of ECAP routes on microstructure and mechanical properties of Mg–Zn–Ca alloy. Mater Sci Eng A. 2010 Jun;527(16–17):4250–6.
[59] Fonda RW, Knipling KE. Texture development in near-α Ti friction stir welds. Acta Mater. 2010;58(19):6452–63.
[60] Fonda RW, Knipling KE. Texture development in friction stir welds. Sci Technol Weld Join. 2011;16(4):288–94.
[61] Gautam PC, Biswas S. Effect of ECAP temperature on the microstructure, texture evolution and mechanical properties of pure magnesium. Mater Today Proc. 2021;44:2914–8.
[62] Biswas S, Singh DS, Beausir B, Toth LS, Suwas S. Thermal response on the microstructure and texture of ECAP and cold-rolled pure magnesium. Metall Mater Trans A Phys Metall Mater Sci. 2015 Jun 1;46(6):2598–613.
[63] Gzyl M, Rosochowski A, Boczkal S, Olejnik L. The role of microstructure and texture in controlling mechanical properties of AZ31B magnesium alloy processed by I-ECAP. Mater Sci Eng A. 2015 Jun 25;638:20–9.
[64] Suh J, Victoria-Hernández J, Letzig D, Golle R, Volk W. Effect of processing route on texture and cold formability of AZ31 Mg alloy sheets processed by ECAP. Mater Sci Eng A. 2016;669:159–70.
[65] Hughes DA, Hansen N. High angle boundaries formed by grain subdivision mechanisms. Acta Mater. 1997;45(9):3871–86.
[66] Tolaminejad B, Dehghani K. Microstructural characterization and mechanical properties of nanostructured AA1070 aluminum after equal channel angular extrusion. Mater Des. 2012;34:285–92.
[67] Cheng W, Tian L, Ma S, Bai Y, Wang H Influence of equal channel angular pressing passes on the microstructures and tensile properties of Mg-8Sn-6Zn-2Al alloy. Materials 2017;10(7):708.